The Astrophysical Journal, 651:713–727, 2006 November 10

REST-FRAME OPTICAL SPECTROSCOPIC CLASSIFICATIONS FOR SUBMILLIMETER GALAXIES[1]

Tadafumi Takata,[2] Kazuhiro Sekiguchi,[3] Ian Smail,[4] Scott C. Chapman,[5] J. E. Geach,[4]
A. M. Swinbank,[4] Andrew Blain,[5] and R. J. Ivison[6,7]
Received 2006 June 19; accepted 2006 July 24

ABSTRACT

We report the results of a systematic near-IR spectroscopic survey using the Subaru, VLT, and Keck Telescopes of a sample of high-redshift ULIRGs mainly composed of submillimeter-selected galaxies. Our observations span the rest-frame optical range containing nebular emission lines such as Hβ, [O III] $\lambda\lambda$4959, 5007, and [O II] λ3727, which are essential for making robust diagnostics of the physical properties. Using the Hα/Hβ emission line ratios, we derive internal extinction estimates for these galaxies similar to those of local ULIRGs: $A_V \sim 2.9 \pm 0.5$. Correcting the Hα estimates of the star formation rate for dust extinction results in rates that are consistent with those estimated from the far-IR luminosity. The majority (>60%) of our sample show spectral features characteristic of AGNs (although this partially reflects an observational bias), with ~65% exhibiting broad Balmer emission lines. A proportion of these sources show relatively low [O III] λ5007/Hβ line ratios, which are similar to those of narrow-line Seyfert 1 galaxies, suggesting low-mass black holes that are rapidly growing. In the subsample of our survey with both [O III] λ5007 and hard X-ray coverage, at least ~60% show an excess of [O III] λ5007 emission, by a factor of 5–10, relative to the hard X-ray luminosity compared to the correlation between these two properties seen in Seyfert galaxies and QSOs locally. From our spectral diagnostics, we propose that the strong [O III] λ5007 emission in these galaxies arises from shocks in dense gaseous regions. Due to sensitivity and resolution limits, our sample is biased to strong-line emitters and hence our results do not yet provide a complete view of the physical properties of the whole high-redshift ULIRG population.

Subject headings: galaxies: active — galaxies: evolution — galaxies: high-redshift — submillimeter

Online material: color figures

1. INTRODUCTION

There is almost irrefutable evidence for an increase in the star formation density with redshift, as demonstrated by emission-line and continuum star formation tracers in wave bands from the ultraviolet to the submillimeter and radio wave bands. This evolution appears to be stronger for tracers that are less sensitive to dust obscuration (e.g., Ivison et al. 2006), suggesting that an increasing proportion of the activity in more distant galaxies may be highly obscured (e.g., Blain et al. 1999, 2002). Indeed, recent results on the mid- to far-infrared emission of luminous but dust-obscured galaxies at high redshift ($z \sim 1$–3) suggest that the origin of their large infrared luminosities is a mix of dust-obscured vigorous star formation and/or dust-enshrouded active galactic nuclei (AGNs; Yan et al. 2005; Houck et al. 2005; Lutz et al. 2005; Desai et al. 2006). In many sources it is likely that both AGNs and star formation contribute to the emission as a result of the close link required between the growth of supermassive black holes (SMBHs) and bulges in massive galaxies (e.g., Borys et al. 2005).

One of the best studied populations of high-redshift, far-infrared luminous galaxies is that identified in the submillimeter wave band using the SCUBA camera (Holland et al. 1999) on the James Clerk Maxwell Telescope (JCMT). Although they span less than an order of magnitude in submillimeter flux, these galaxies are responsible for much of the energy density in the submillimeter background (Barger et al. 1998; Hughes et al. 1998; Smail et al. 2002; Cowie et al. 2002; Scott et al. 2002). The faintness of these obscured galaxies in the optical wave band has made it difficult to obtain precise redshifts (e.g., Simpson et al. 2004), although some progress has been made using ultraviolet/blue spectrographs (Chapman et al. 2003a, 2005). The median redshift for submillimeter galaxies (SMGs) with 850 μm fluxes of $\gtrsim$5 mJy is $\langle z \rangle \sim 2.2$ (Chapman et al. 2003a, 2005). The submillimeter and radio fluxes of these systems indicate that their bolometric luminosities are $\gtrsim 10^{12} L_\odot$ (Kovacs et al. 2006), confirming that they are examples of high-redshift ultraluminous infrared galaxies (ULIRGs).

This population provides critical constraints on models of galaxy formation and evolution. In particular, if the bolometric emission from SMGs is powered solely by star formation, then these galaxies form about half of the stars seen in the local universe (Lilly et al. 1999). However, it appears likely that both AGNs and star formation activity contribute to the immense far-infrared luminosities of these systems, although it has been difficult to disentangle the precise balance between these two energy sources.

[1] Based partly on data collected at Subaru Telescope and obtained from the SMOKA science archive at the Astronomy Data Analysis Center, which are operated by the National Astronomical Observatory of Japan. Based partly on the data collected with the ESO VLT-UT1 Antu Telescope [074.B-0107(A)]. Based partly on data obtained at the Keck Observatory, which is operated as a scientific partnership among the California Institute of Technology, the University of California, and the National Aeronautics and Space Administration. The observatory was made possible by the generous financial support of the W. M. Keck Foundation.

[2] Astronomy Data Center, National Astronomical Observatory of Japan, 2-21-1 Osawa, Mitaka, Tokyo 181-8588, Japan; tadafumi.takata@nao.ac.jp.
[3] Subaru Telescope, National Astronomical Observatory of Japan, 650 North A'ohoku Place, Hilo, HI 96720.
[4] Institute for Computational Cosmology, Department of Physics, Durham University, South Road, Durham DH1 3LE, UK.
[5] Astronomy Department, California Institute of Technology, MS 105-24, Pasadena, CA 91125.
[6] Astronomy Technology Center, Royal Observatory, Blackford Hill, Edinburgh EH9 3HJ, UK.
[7] Institute for Astronomy, University of Edinburgh, Blackford Hill, Edinburgh EH9 3HJ, UK.

Recent sensitive X-ray analysis suggests that star formation is likely to be the dominant source of the bolometric luminosity in SMGs (Alexander et al. 2005a, 2005b). Further evidence suggests that it is plausible to identify SMGs as the progenitor of massive elliptical galaxies at the present day, based on their large gas, stellar, and dynamical masses (Neri et al. 2003; Greve et al. 2005; Tacconi et al. 2006; Smail et al. 2004; Borys et al. 2005; Swinbank et al. 2004, 2006). Furthermore, combining the X-ray constraints on the AGN within this population with the typical mass estimates suggests that SMGs are the sites of coeval growth of stellar bulges and central black holes (Borys et al. 2005).

Rest-frame optical emission lines provide a powerful tool to investigate many fundamental properties of galaxies, such as star formation rates (SFRs), power sources, internal extinction, and metallicity. Swinbank et al. (2004) conducted a systematic near-infrared spectroscopic survey of 30 SMGs to investigate their SFRs and metallicities and the kinematics of the emission-line gas. However, the wavelength coverage was limited to the region around Hα and so they did not include several emission lines at shorter wavelengths, such as Hβ and [O III] $\lambda\lambda$4959, 5007, which are useful for evaluating internal extinction and metallicity or determining the power source.

We present in this paper the results from a near-infrared spectroscopic survey of redshifted [O III] $\lambda\lambda$4959, 5007, Hβ, and [O II] λ3727 lines for a sample of far-infrared luminous galaxies. The sample is composed of SMGs and optically faint radio galaxies (OFRGs), at $z \sim 1$–3.5. Chapman et al. (2004) and Blain et al. (2004) claim that high-redshift OFRGs are ULIRGs, with similar bolometric luminosities to SMGs but warmer characteristic dust temperature, resulting in them being undetectable in the submillimeter wave band. We use Hα/Hβ emission line ratios to derive the dust extinction in these systems and then employ these estimates to derive extinction-corrected SFRs from the Hα luminosities. In addition, we also use X-ray observations of these objects to compare the strength of the [O III] λ5007 emission to their X-ray emission and so investigate the power of the AGNs in these galaxies. We adopt cosmological parameters of $H_0 = 72\ \mathrm{km\ s^{-1}\ Mpc^{-1}}$, $\Omega_M = 0.3$, and $\Omega_\Lambda = 0.7$ throughout.

2. OBSERVATION AND DATA REDUCTION

Our sample was selected from the catalogs of SMGs and OFRGs in Chapman et al. (2004, 2005). We chose SMGs/OFRGs in the redshift ranges $z = 2.05$–2.56 and $z = 1.28$–1.68, where nebular emission lines such as [O II], Hβ, [O III], and/or Hα are redshifted into clear parts of the *J*, *H*, and *K* bands, respectively. In total, 22 targets were observed using the OHS spectrograph on Subaru, ISAAC on the VLT, or NIRSPEC on Keck. The log of the observations is given in Table 1.

2.1. *Subaru OHS Observations and Data Reduction*

The majority of our spectroscopic observations were taken with the OH Suppression Spectrograph (OHS; Iwamuro et al. 2001) with the Cooled Infrared Spectrograph and Camera for OHS (CISCO; Motohara et al. 2002) attached to the Nasmyth focus of Subaru Telescope (Iye et al. 2004). Observations were obtained on the nights of 2004 April 6 and 7, 2004 June 24–25, and 2005 February 14–16. Sky conditions were photometric on all of these nights with typical seeing 0.″5–0.″7 at 1.6 μm. We used a slit width of 0.″95, which gives a resolution of $\Delta\lambda/\lambda \sim 200$ ($\sim$1400 km s^{-1}), and used the "SP4" dither pattern, which shifts the object along the slit to four positions in one sequence. After completing each observation, we observed bright A- or F-type stars with the same configuration as the science observation to calibrate the extinction and sensitivity variation with wavelength. During each night we observed at least two photometric standard stars selected from the UKIRT Faint Standards catalog (Hawarden et al. 2001). We used FS 27 and FS 127 for the observations taken in 2004 April, FS 23 and FS 30 in 2004 June, and FS 133 and FS 127 in 2005 February.

The data reduction was performed in the standard manner using custom scripts in IRAF and some C programs provided by the OHS/CISCO instrument teams. First, we subtracted the sky background using the object frames at different dither positions. Next, we fitted the skyline residuals using two-dimensional polynomials and subtracted these from the data. We then shift-and-added the images from the different dithering positions, using a median combine. As the instrument is stable, wavelength calibration was performed using the nominal conversion of pixel coordinates to wavelength. To confirm the stability of the wavelength solution, we analyzed argon calibration lamp exposures taken during our runs and checked for systematic shifts in wavelength. We found typical systematic shifts of 7–9 Å ($\sim$0.05%), which is ignorable in our analysis due to the low resolution of our spectra. Extinction, sensitivity, and photometric calibration were performed by dividing the calibrated spectra with those of the bright A- or F-type standard-star observations after fitting the stellar spectra with models.

2.2. *VLT ISAAC Observations and Data Reduction*

We conducted observations of four SMGs and one OFRG using the ISAAC spectrograph on the 8 m VLT on 2004 November 22–23 (Table 1). ISAAC was used in medium-resolution mode, which provides spectral resolution of 3000 ($\sim$100 km s^{-1}). Seeing was steady at $\sim$0.″8 over the course of the observations, and the observations were taken with a standard 10″ ABBA chop. Preliminary data reduction was performed using the ECLIPSE[8] pipeline, using flat fields generated from night calibrations taken after each observation, and wavelength calibration from a solution using the OH skylines. The remaining flux calibration was achieved in IRAF, using corresponding *Hipparcos* standard stars observed throughout the observing run and near-infrared fluxes derived from the Two Micron All Sky Survey (2MASS) catalog.

2.3. *Keck NIRSPEC Observations and Data Reduction*

The observations of SMM J09431+4700 (H6/H7) and SMM J131201.17+424208.1 were taken on 2004 April 8 in photometric conditions and 0.″8 seeing using the NIRSPEC spectrograph on Keck. These observations employed the standard ABBA configuration to achieve sky subtraction. Each exposure was 600 s in length and the total integration time was 2400 s. The data were reduced using the WMKONSPEC package in IRAF. We remapped the two-dimensional spectra using linear interpolation to rectify the spatial and spectral dimensions. After subtracting pairs of nod positions (the nod was 20″ along the slit), residual sky features were removed in IDL using sky regions on either side of the object spectrum. For the wavelength calibration we used an argon arc lamp. The output pixel scale is 4.3 Å pixel^{-1}, and the instrumental profile has an FWHM of 15 Å (measured from the widths of the skylines), which corresponds to $\sim$200 km s^{-1}. We used FS 27 for photometric calibration.

3. RESULTS

3.1. *General Spectral Features*

We show all of our spectra in Figure 1. We identified emission lines in 20 spectra out of 22 targets that were observed. Most of

[8] Ver. 4.9-0; see http://www.eso.org/projects/aot/eclipse.

TABLE 1
Observation Log and Basic Parameters

Object	t_{exp} (s)	Observation Date	Bands	L_{FIR}[a] (10^{12} $L_\odot$)	F_{HX}[b] (10^{16} ergs s^{-1} cm^{-2})	Comment
Subaru OHS Observation						
SMM J123549.44+621536.8	7200	2004 Apr 6	J and H	$6.8^{+1.5}_{-1.1}$[c]	12.0±1.4[d]	
SMM J123606.85+621021.4	7200	2005 Feb 15	J and H	$8.7^{+1.8}_{-1.2}$[c]	7.4±1.4[d]	
SMM J123622.65+621629.7	7200	2004 Apr 7	J and H	$9.0^{+1.9}_{-2.0}$[c]	11.0±1.4 [d]	
SMM J123635.59+621424.1	7200	2005 Feb 16	J and H	$7.5^{+1.5}_{-1.5}$[c]	25.0±1.4[d]	
SMM J123716.01+620323.3	4000	2005 Feb 16	J and H	$6.3^{+1.0}_{-1.0}$[e]	74.0±1.4[d]	
SMM J123721.87+621035.3	7200	2004 Jun 24	J and H	$0.43^{+0.09}_{-0.09}$[e]	21.0±1.4[d]	
SMM J131215.27+423900.9	600	2005 Feb 16	J and H	$13.9^{+0.5}_{-2.5}$[c]	190.0±23.0[f]	
SMM J131222.35+423814.1	2000	2004 Jun 25	J and H	$12.7^{+2.5}_{-2.5}$[g]	120.0±20.0[f]	
SMM J163639.01+405635.9	7200	2004 Jun 24	J and H	$5.5^{+1.9}_{-1.5}$[c]	<22.0[h]	
SMM J163650.43+405734.5	7000	2003 May 18	J and H	$50.5^{+15.0}_{-15.8}$[c]	<22.0[h]	Smail et al. (2003)
MM J163655+4059	3600	2004 Apr 7	J and H	$10.9^{+2.2}_{-3.8}$[c]	150.0±21.0[h]	
SMM J163706.51+405313.8	7200	2004 Apr 6	J and H	$7.2^{+4.2}_{-3.0}$[c]	<22.0[h]	
SMM J221733.02+000906.0	3000	2004 Jun 24	J and H	$1.9^{+0.4}_{-0.4}$[g]	<28.0[i]	
SMM J221733.79+001402.1	7200	2004 Jun 25	J and H	$4.9^{+1.9}_{-2.6}$[c]	<28.0[i]	
VLT ISAAC Observation						
SMM J02399−0134	4500	2004 Nov 24, 25	J	$6.5^{+1.3}_{-1.3}$[j]	32.0±5.0[k]	
	2400	2004 Nov 25	z	...	...	
SMM J030227.73+000653.5	6000	2004 Nov 23	J	$5.8^{+2.4}_{-0.8}$[c]	60.0±10.0[l]	
RG J030257.94+001016.3	4500	2004 Nov 23	H	$7.7^{+1.4}_{-1.4}$[c]	60.0±10.0[l]	
SMM J105702.50−033602.6	4500	2004 Nov 23	H	$5.0^{+1.0}_{-1.0}$[m]	<10.0[m]	
SMM J221737.39+001025.1	9000	2004 Nov 23, 24	K	$21.0^{+4.2}_{-4.2}$[g]	<28.0[i]	
	6000	2004 Nov 25	H	...	...	
Keck NIRSPEC Observation						
SMM J09431+4700 (H6)	2400	2004 Apr 8	K	$15.0^{+3.0}_{-3.0}$[n]	<13.0[n]	
SMM J09431+4700 (H7)	2400	2004 Apr 8	K	$15.0^{+3.0}_{-3.0}$[n]	<13.0[n]	
SMM J131201.17+424208.1	2400	2004 Apr 8	K	$20.2^{+4.0}_{-4.0}$[g]	52.8±40.0[f]	
From Literature						
SMM J04431+0210	...	...	...	$3.5^{+1.5}_{-1.5}$[j]	...	Frayer et al. (2003)
SMM J14011+0252 (J1)	...	...	...	$6.8^{+2.5}_{-2.5}$[j]	<44.0[o]	Motohara et al. (2005)
SMM J163658.19+410523.8	...	...	...	$10.9^{+2.2}_{-3.8}$[c]	<22.0[h]	Simpson et al. (2004)

[a] FIR luminosity.
[b] Hard X-ray flux.
[c] Swinbank et al. (2004).
[d] Alexander et al. (2003).
[e] Alexander et al. (2005a).
[f] Mushotzky et al. (2000).
[g] Smail et al. (2004).
[h] Manners et al. (2003).
[i] Basu-Zych & Scharf (2004).
[j] Smail et al. (2002).
[k] Bautz et al. (2000).
[l] Waskett et al. (2004).
[m] van Dokkum et al. (2004).
[n] Ledlow et al. (2002).
[o] Fabian et al. (2000).

the SMGs show weak Hβ emission, but many show strong (and sometimes broad and distorted) profiles in [O III] $\lambda\lambda$4959, 5007. Some of our spectra show additional emission lines of [Ne III], [Ne V], and [O I] λ6300, which are common in AGNs. Five of the SMGs from our sample [SMM J09431+4700 (H6), SMM J123549.44+621536.8, SMM J123716.01+620323.3, SMM J163639.01+405635.9, and SMM J163650.43+405734.5] display spatially extended structures ($\geq 1''.0$) in either the [O III] λ5007 or Hα emission line (Fig. 2; for evidence of the spatial extension in SMM J163650.43+405734.5 see Smail et al. 2003; Swinbank et al. 2005).

3.2. *Comments on Individual Objects*

Several of our observations are particularly noteworthy, and we discuss them here.

3.2.1. *SMM J02399−0134*

This galaxy is identified as a submillimeter source associated with a spiral galaxy at $z = 1.06$, which shows features typical of a Seyfert 1 (Smail et al. 1997, 2002; Soucail et al. 1999). The strong and featureless continuum, together with the spatially compact emission line flux, indicates AGN activity, an interpretation that is further supported by the detection of this source in hard X-rays by Bautz et al. (2000). Our spectrum shows at least two peaks in the Hα emission line with FWHM$_{rest}$ $\sim$ 200−400 km s^{-1}, consistent with these lines arising from independent components within the system. If we force fit a single Gaussian profile to the Hα emission, we determine FWHM$_{rest}$ = 1530 ± 500 km s^{-1}, which if it arises from an AGN is narrower than typical Seyfert 1 galaxies, although broader than Seyfert 2 galaxies ($\sim$500 km s^{-1}). This source is also detected in a CO observation by Greve et al. (2005) with a double-peaked profile with an FWHM of 780 ± 60 km s^{-1} and a separation between the two peaks of $\sim$400 km s^{-1}, consistent within the errors with our measurements from Hα. We therefore choose to interpret the double-peaked Hα line as evidence for a merger or interaction in this system, with any AGN-produced broad component undetected in our spectrum.

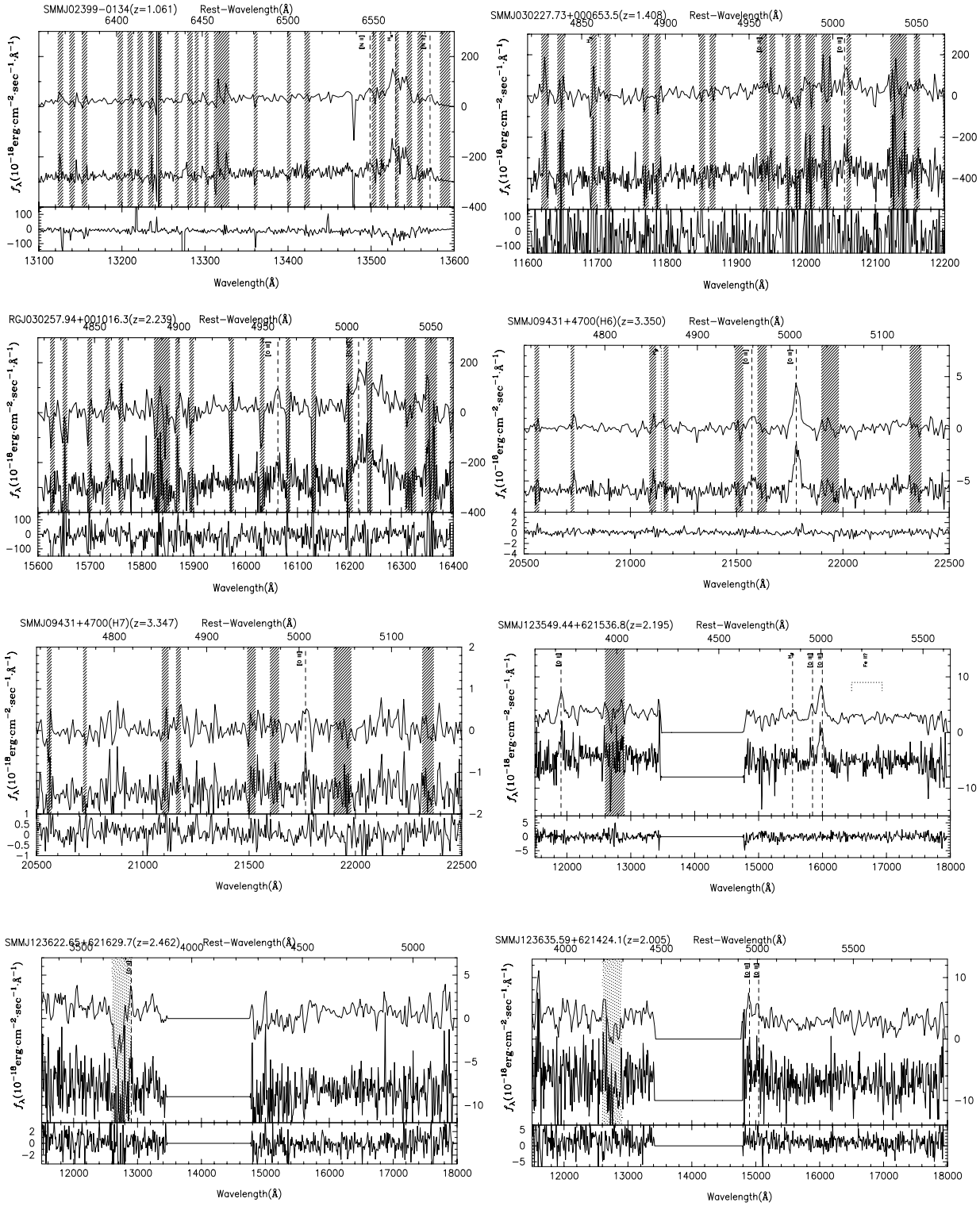

FIG. 1.—Near-infrared spectra of the galaxies in our sample. The upper spectrum in each panel is smoothed to the instrumental resolution, the middle spectrum shows the raw data, and the lower spectrum illustrates the sky emission as a function of wavelength. The dashed and dotted lines show the detected emission lines with >4 σ and 2–4 σ significance, respectively. The upper axis gives the rest-frame wavelength scale at the source redshift. The shaded regions are areas affected by strong sky emission or absorption.

3.2.2. *SMM J09431+4700*

This source was discovered by Cowie et al. (2002) and has been identified with two distinct microjansky radio counterparts: H6 and H7 (Ledlow et al. 2002). These are lensed sources, lying behind a massive cluster Abell 851 at $z = 0.41$ although the amplification is modest: 1.3 times. The redshift for H6 was measured by Ledlow et al. (2002) as $z = 3.349$ from Lyα; H7 was not observed. The rest-frame UV properties of H6 suggest that it hosts an AGN with spectral features similar to a narrow-line Seyfert 1 (Ledlow et al. 2002). We placed the NIRSPEC slit across both radio components and detected [O III] λ5007 emission from both

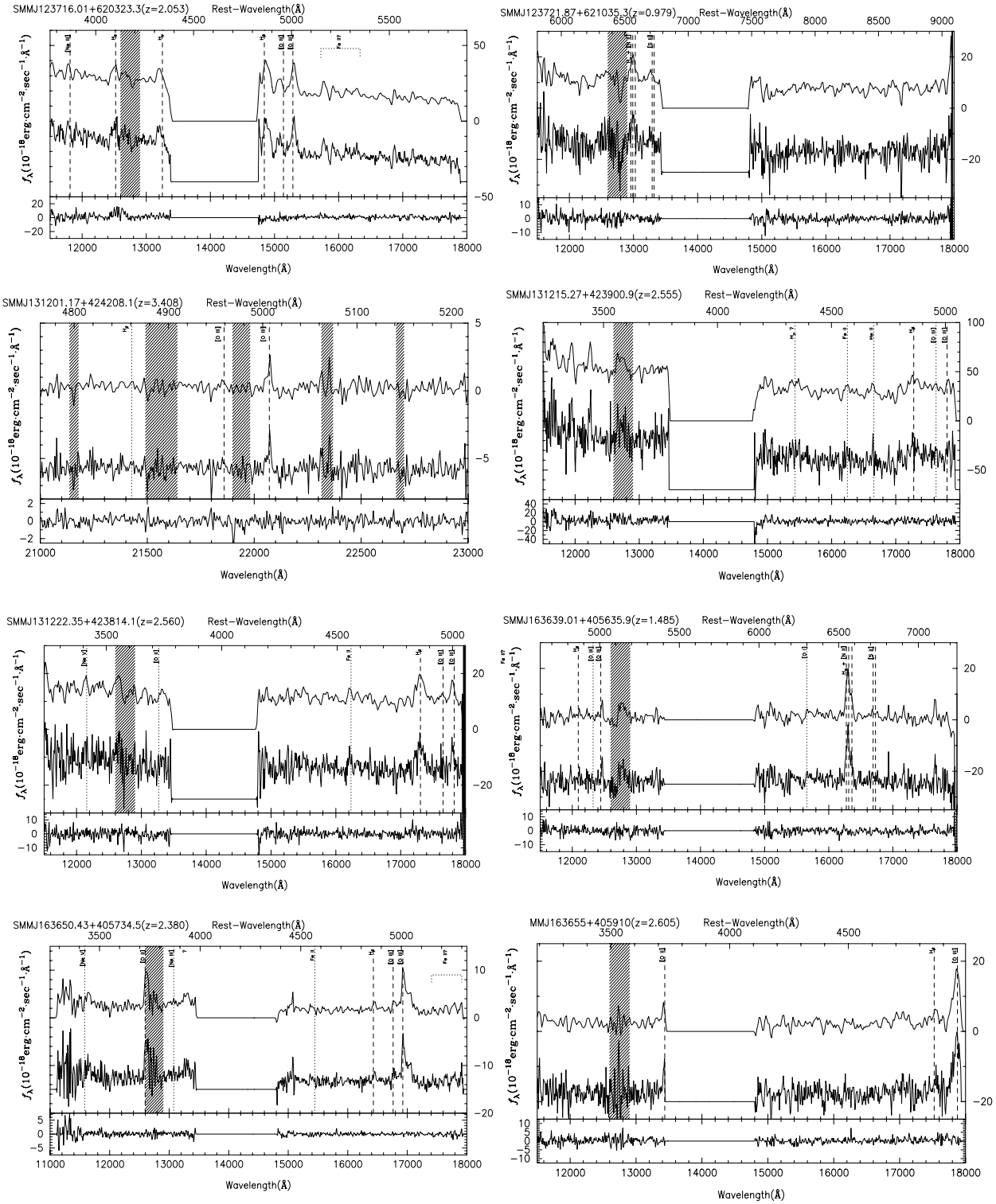

FIG. 1.—*Continued*

sources at redshifts of $z = 3.350$ and 3.347 for H6 and H7, respectively. We also detected narrow ($\mathrm{FWHM_{rest}} \sim 350$ km s^{-1}) Hβ emission from H6. The [O III] λ5007 emission from H6 is spatially extended (>2″ or 14.5 kpc; Fig. 2) but has no significant velocity gradient across ~8 kpc in projection. No hard X-ray emission was detected with the upper limits on $f_{2-10\,\mathrm{keV}}$ as $\sim 1 \times 10^{-15}$ ergs s^{-1} cm^{-2} (Ledlow et al. 2002). CO line emission is also detected by Neri et al. (2003) and Tacconi et al. (2006) based on our rest-frame optical redshift, originating from H7 at $z = 3.346$. Millimeter continuum emission has been seen from H6, but assuming that the gas reservoir is at the redshift we find from [O III] λ5007, the gas mass of the AGN-dominated component, H6, is a factor of a few lower than that of H7.

3.2.3. *SMM J123549.44+621536.8*

This source has apparent double-peaked, narrow (<1500 km s^{-1}) emission lines in [O II] λ3727 and [O III] $\lambda\lambda$4959, 5007, with the two components spatially offset by ~0.″2. The one-dimensional

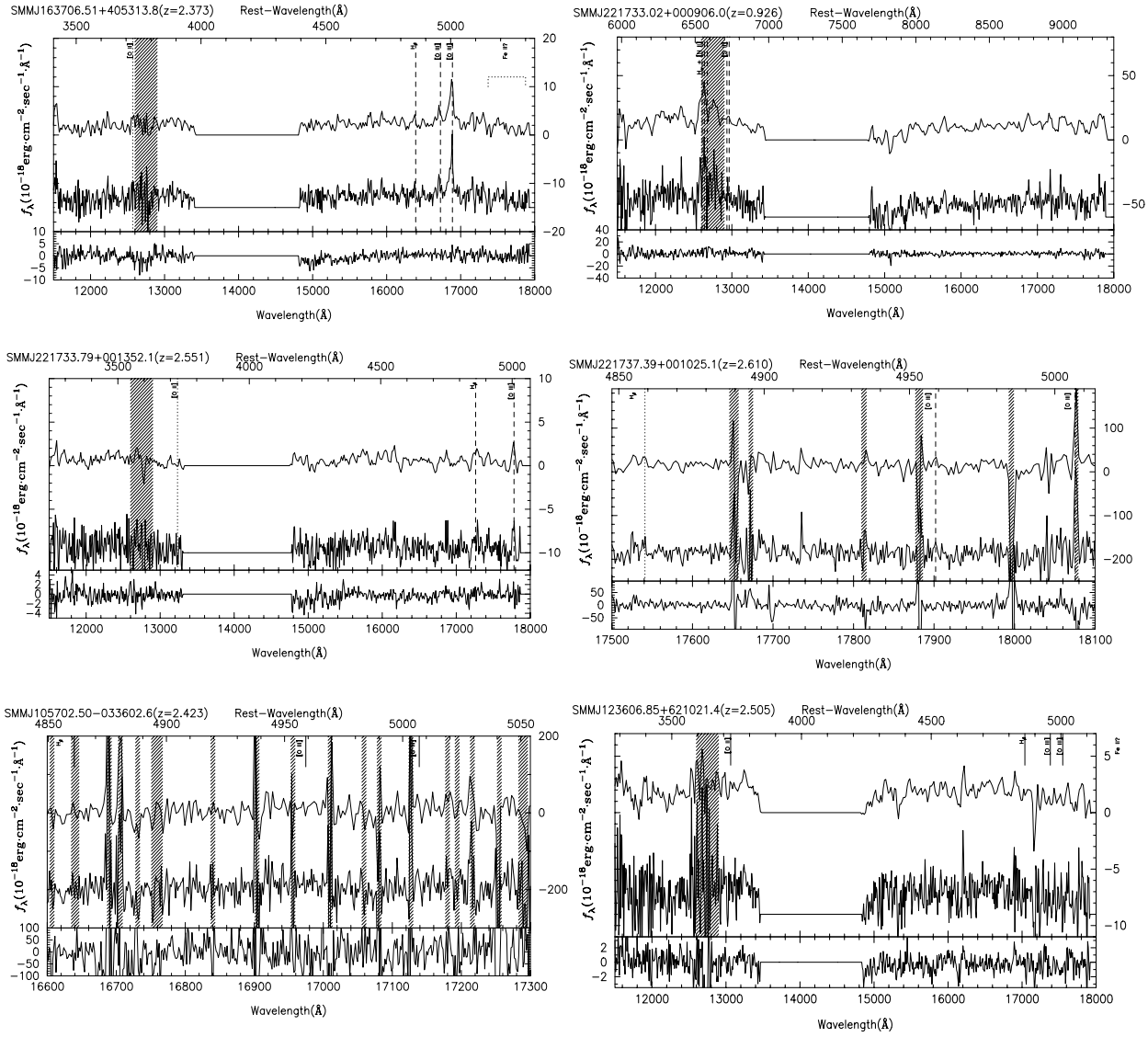

FIG. 1.—*Continued*

spectra also show signs of broad Hβ emission at $z = 2.195 \pm 0.005$ with an FWHM of 2100 $\pm$ 500 km s^{-1}. Both the [O III] λ5007 and the [O II] λ3727 emissions are spatially extended with faint wings on scales of approximately 1″ (∼8 kpc; see Fig. 2). There may also be a very weak, broad multiplet of Fe II $\lambda\lambda$5190, 5320 (Fig. 1), potentially indicating the presence of the narrow-line Seyfert 1 (NLS1) type AGN component (Osterbrock & Pogge 1985; Goodrich 1989). This is consistent with the results of Alexander et al. (2005a), which indicated the presence of a heavily obscured AGN with $N_{\rm H} \sim 10^{24}$ cm^{-2} based on their X-ray spectral analysis. The spatial extension in the bright core of the [O III] λ5007 likely indicates merging components or rotation along the slit, while the extended wings may reflect "superwind" activity.

3.2.4. *SMM J123716.01+620323.3*

This source is very bright in the optical ($R_{\rm AB} = 20.2$) with a redshift of $z = 2.053 \pm 0.005$, and it was classified as a QSO by Chapman et al. (2005) based on the broad rest-frame UV emission lines and comparable luminosities in rest-frame optical and far-infrared wavelength, which exceed 10^{45} ergs s^{-1}. The source has also been detected in hard X-rays by Alexander et al. (2005a). Our spectrum shows several hydrogen Balmer lines such as Hβ, Hδ, and Hγ with broad FWHM$_{\rm rest}$ (∼2200–2700 km s^{-1}) and the [O III] $\lambda\lambda$4959, 5007 doublet with FWHM$_{\rm rest}$ of ∼2200 km s^{-1}. We also detected the [Ne III] and several Fe II lines at 3–4 σ significance. The rest-frame optical spectrum is dominated by continuum emission without stellar absorption features, suggesting a large contribution from the AGN component to the total rest-frame optical flux. The [O III] λ5007 emission lines are wide (FWHM$_{\rm rest}$ ∼ 2000 km s^{-1}) and spatially extended (∼1.″5, 12 kpc), indicating dynamically active gas motion (Fig. 2). The estimated hydrogen column density from the X-ray spectral analysis is relatively low ($N_{\rm H} \sim 10^{22.5}$ cm^{-2}), which implies that the AGN does not suffer from large extinction. It should be noted that the redshift based on the rest-frame UV emission lines is 2.037 $\pm$ 0.002, which is blueshifted by 1600 $\pm$ 700 km s^{-1} from the redshift indicated by the rest-frame optical nebular emission line. This velocity offset may arise due to broad Lyα emission that may be affected by dust extinction and resonance scattering.

3.2.5. *SMM J131222.35+423814.1*

This source is another example of an NLS1-type AGN. It lies at $z = 2.560$ and our spectrum displays broad Hβ emission, with

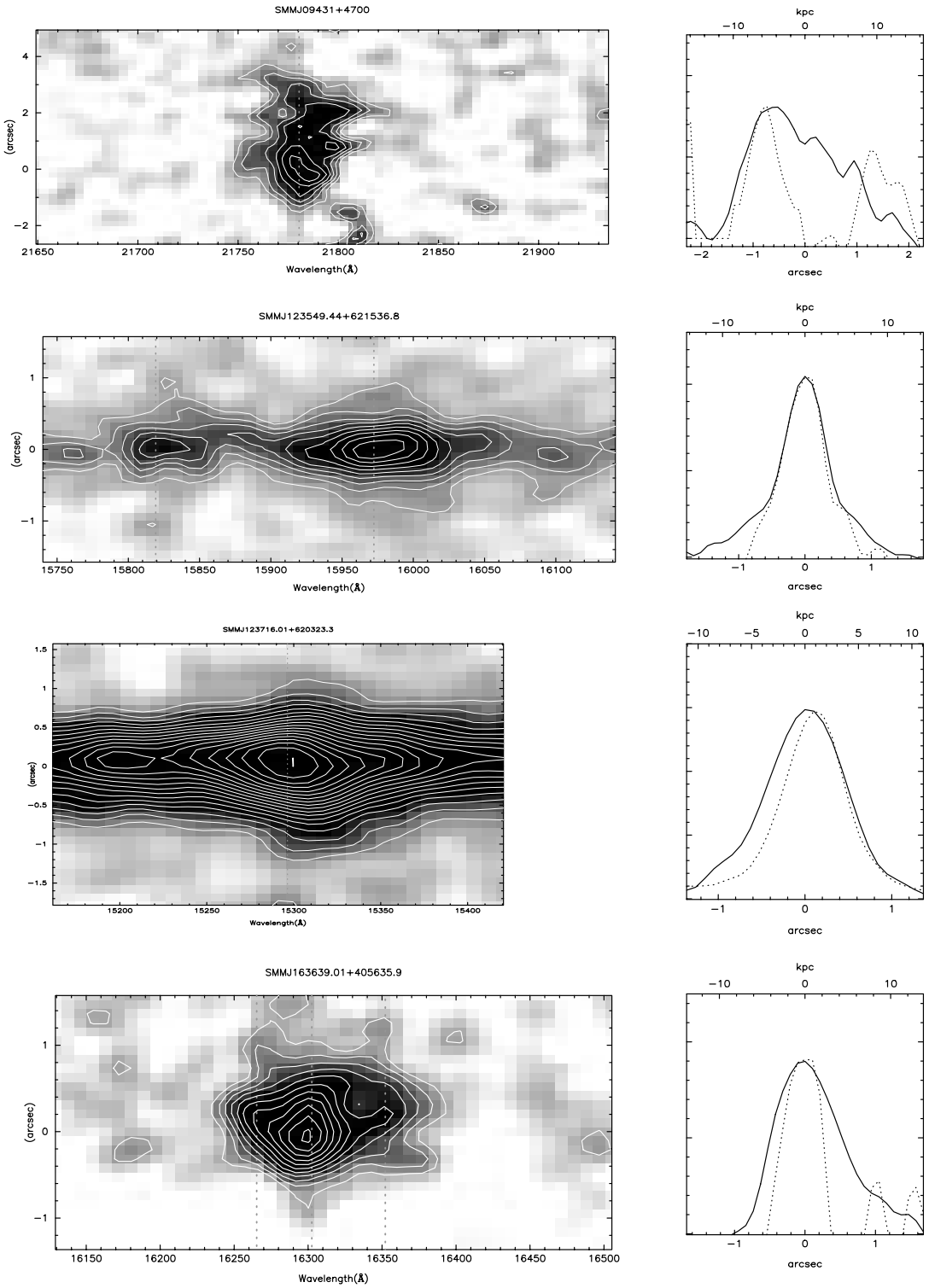

FIG. 2.—Position-wavelength maps (*left*) and slit profiles (*right*) for sources with spatially extended [O III] λ5007 or Hα lines. From top to bottom, these are SMM J09431+4700 (H6), SMM J123549.44+621536.8, SMM J123716.01+620323.3, and SMM J163639.01+405635.9. In the position-wavelength maps, the contours are spaced from 2 σ at 1 σ intervals. The dotted lines display the expected wavelengths of the [O III] $\lambda\lambda$4959, 5007, Hα, or [N II] lines at the redshifts listed in Table 2. In the slit profiles, the solid and dotted lines show the light profile for the emission lines and neighboring continuum, respectively. The emission-line profiles consist of [O III] λ5007 emission for SMM J09431+4700 (H6), SMM J123549.44+621536.8, and SMM J123716.01+620323.3 and Hα emission for SMM J163639.01+405635.9. The width used for constructing the emission profiles corresponds to 1000 km s^{-1} in their rest frame. The spatially extended emission in [O III] λ5007 and Hα, relative to the neighboring continuum, is likely to represent outflows of gas from these systems on scales of $\sim$10 kpc. [*See the electronic edition of the Journal for a color version of this figure*.]

$FWHM_{rest} \sim 2600 \pm 1000$ km s^{-1} and a low [O III] λ5007/Hβ ratio ($0.46^{+0.35}_{-0.28}$). This source has Lyα [C IV] and He II emission lines in the rest-frame UV spectrum and was classified as a QSO by Chapman et al. (2005). The rest-frame optical emission is dominated by very strong continuum emission without stellar absorption lines, supporting the presence of a luminous AGN component. Unfortunately, there is no coverage of Hα emission for this object and so we could not constrain the internal extinction. The [Ne V] line (which is a very clean indicator of AGN activity; Osterbrock 1989) is detected. Furthermore, this source was detected by the X-ray imaging by Mushotzky et al. (2000), confirming the presence of a luminous AGN in the source.

3.2.6. *SMM J163639.01+405635.9*

This source is a good example of a heavily extincted starburst in an SMG and was recently discussed by Swinbank et al. (2006). This $z = 1.485$ galaxy has a weak Hβ emission line with Hα/H$\beta = 10.4^{+29.6}_{-4.9}$. The H$\alpha$ and [O III] λ5007 emission lines are spatially extended ($\sim$1.″2 or 10 kpc; Fig. 2). There is only an upper limit on its X-ray emission, $f_{2-8\,\mathrm{keV}} < 2.2 \times 10^{-15}$ ergs s^{-1} cm^{-2} from Manners et al. (2003), which does not strongly constrain the presence of a luminous AGN given the possibility of substantial absorption (e.g., Alexander et al. 2005a). The possible detection of the [O I] λ6300 emission line may hint at the presence of an AGN, although the line ratios of [O I] λ6300/H$\alpha \sim 0.1$ and [O III] λ5007/H$\beta \sim 3.5$ can be explained by relatively highly ionized starburst nebulae (Osterbrock 1989).

3.2.7. *MM J163655+405910*

This heavily obscured AGN at $z = 2.605$ was found in the MAMBO survey of Greve et al. (2004) (and is also called N2 1200.18) and was detected in X-ray imaging with *Chandra* (Manners et al. 2003). It has broad ($FWHM_{rest} \sim$ 2000–2500 km s^{-1}) emission lines of Lyα, [C IV], and Hα in the rest-frame UV and optical wavelengths, with a high [O I] λ6300/Hα ratio ($\sim$0.3; Willott et al. 2003; Swinbank et al. 2006), which is typical of AGNs (Osterbrock 1989). Our data also show asymmetric Hβ and [O III] λ4959 emission line profiles, which exhibit "blue wings" in their profiles. Such profiles have been interpreted as evidence for wind activity from the AGN, although contribution from other components is possible (Swinbank et al. 2006).

3.2.8. *SMM J221737.39+001025.1*

Our ISAAC spectrum shows strong, narrow Hα, Hβ, [O III] $\lambda\lambda$4959, 5007, and [N II] emission lines at a redshift of $z = 2.610$ ($FWHM_{rest}$ of Hβ is 290 ± 50 km s^{-1}). To investigate the rest-frame optical properties, we retrieved an archival i'-band image taken with Subaru Telescope's Prime Focus Camera (Suprime-Cam) using SMOKA.[9] The image shows an elongated structure, $\sim$1.″3, toward the northwest, and the spectrum was taken with the slit aligned along the major axis of this source. We identify two separate Hα emission lines with a velocity offset of $\sim$300 km s^{-1} and a spatial offset $\sim$0.″2–0.″3 ($\sim$2 kpc). These suggest that the system is a merger. The Hα and Hβ emission lines do not show asymmetric profiles or detectable broad-line components.

3.3. *Composite Spectra*

Since many of our individual spectra have modest signal-to-noise ratio, we have also constructed several composite spectra to investigate the general properties of subsets of the SMG population.

[9] See http://smoka.nao.ac.jp.

We create the composite spectra by deredshifting each spectrum based on redshifts measured from the [O III] λ5007 lines, subtracting continuum emission using a first-order spline fit, and averaging all of the spectra with 3 σ clipping after normalizing by [O III] λ5007 flux. We smoothed the higher resolution spectra taken at Keck and VLT to match the low-resolution Subaru spectra before stacking. Either stacking the spectra with weights based on their individual signal-to-noise ratio or an unweighted stack does not alter any of the conclusions below. We derive a composite spectrum for those sources that show QSO signatures ("QSO," i.e., classified as QSO) and for those galaxies that individually show signs of an AGN in their optical spectra ("OPT-AGN," i.e., those classified as AGNs in the "Class" column under the "OPT" category in Table 2). The former is made from only three individual spectra, while the latter comes from nine spectra. The resulting composite spectra are shown in Figure 3. We do not make a composite of starburst ("SB") sources since there are only two sources in our sample classified as "SB" or intermediate ("Int") from their rest-frame optical spectra. The details of the classification are discussed in § 4.1.

The emission lines of Hβ and [O III] $\lambda\lambda$4959, 5007 are clearly seen in both of the composite spectra. In addition, in the "QSO" spectrum, many strong lines are visible, including [Ne III] λ3869 and several Fe II lines at $\lambda = 4570$, 5167, and 5200–5360 Å, although the [O II] λ3727 line is only marginally detected. By fitting a Gaussian to the Hβ and [O III] $\lambda\lambda$4959, 5007 emission lines, we measure the $FWHM_{rest}$ of Hβ as $\sim 3200 \pm 1000$ km s^{-1} after correction for the instrumental resolution. This is $\sim$2000 km s^{-1} lower than the average FWHM of QSOs at $z = 0.1$–2.1 (Jarvis & McLure 2006). The [O III] λ5007/Hβ ratio is $0.36^{+0.33}_{-0.18}$. All of these spectral features are typical of type 1 AGNs studied locally.

On the other hand, in the composite "OPT-AGN" spectrum, a Gaussian profile fit to the Hβ emission line yields $FWHM_{rest}$ of 1730 ± 500 km s^{-1} (it should be noted that the Hβ line fit is not improved by including a narrow-line component due to the low spectral resolution of our spectra) and [O III] λ5007/Hβ ratio of $3.2^{+1.0}_{-0.6}$, and the [O II] λ3727 line is well detected. The Hβ line, which is broader than typical type 2 AGNs, and relatively low [O III] λ5007/Hβ line ratio are similar to those of local NLS1 galaxies (although by definition these should have [O III] λ5007/H$\beta <$ 3.0). The Fe II emission lines, which are one of the characteristic features seen in local NLS1 galaxies, are marginally detected with $\sim 2\,\sigma$ features seen around 5200 Å in the spectrum, and we can see some marginal detections in individual spectra (SMM J123549.44+621536.8, SMM J123635.59+621424.1, SMM J163650.43+405734.5, and SMM J163706.51+405313.8), all of which have broad Hβ emission of $FWHM_{rest} \sim 2000$ km s^{-1} (Fig. 1). The resultant spectrum is consistent with a scenario where the rest-frame optical spectra classified as "AGN" in the UV in reality comprise two types: one has relatively broad ($\sim$2000 km s^{-1}) FWHM for the Hβ lines, and the other has narrow Hβ lines with a relatively high [O III] λ5007/Hβ ratio, typical of type 2 AGNs. There are clearly differences in the extinction of the circumnuclear region of these two types of objects implied by the difference in luminosity and spectroscopic properties of the rest-frame UV emission, although there is no systematic difference in the Hα/Hβ ratio we measure for them.

4. DISCUSSIONS

4.1. *Emission-Line Diagnostics*

In Figure 4 we plot the observed [O III] λ5007/Hβ versus [N II]/Hα emission line ratios of the 13 galaxies in our sample for which we have secure Hα detections and some information about

TABLE 2
SUMMARY OF RESULTS

OBJECT	z [a]	Hα FLUX (10^{-16} ergs cm^{-2} s^{-1})	Hβ FLUX (10^{-16} ergs cm^{-2} s^{-1})	[O III] λ5007 FLUX (10^{-16} ergs cm^{-2} s^{-1})	[O III] λ4959 FLUX (10^{-16} ergs cm^{-2} s^{-1})	[O II] λ3727 FLUX (10^{-16} ergs cm^{-2} s^{-1})	CLASS UV	CLASS Hα	CLASS Opt	REST FWHM$_{H\beta}$ (km s^{-1})	COMMENT
SMM J02399−0134	1.061[b]	75.8±15.0	<11.0	<11.0	<11.0	...	AGN	AGN	...	1530±500[c]	
SMM J030227.73+000653.5	1.408	15.2±2.0	1.9±1.1	10.7±3.2	7.2±2.6	...	SB	AGN	AGN	<100	
RG J030258.94+001016.3	2.239	1.8±0.5	<0.3	9.2±2.1	0.85±0.30	...	Int	AGN	AGN	...	
SMM J09431+4700 (H6)	3.350	...	0.3±0.2	1.7±0.3	0.7±0.4	...	SB	...	SB?	350±50	Extended [O III] λ5007
SMM J09431+4700(H7)	3.347	...	<0.15	0.5±0.1	<0.15	...	...	...	...	...	
SMM J105702.50−033602.6	2.423[c]	0.6±0.2	<0.19	<0.19	<0.19	...	...	SB	...	...	van Dokkum et al. (2004); miss the slit?
SMM J123549.44+621536.8	2.195	15.0±1.0	1.6±1.0	6.4±1.3	1.9±0.8	2.9±0.8	SB	Int	AGN	2150±500	[O III] λ5007 double peaks and extended
SMM J123606.85+621021.4	2.505[c]	2.0±0.3	<0.043	<0.043	<0.043	<0.043	SB	Int	...	...	Slit on companion object?
SMM J123622.65+621629.7	2.462[b]	3.4±0.6	<0.8	<0.8	<0.8	2.1±0.5	SB	SB	...	...	
SMM J123635.59+621424.1	2.005	11.1±1.2	...	2.0±0.6	2.4±0.5	...	AGN	AGN	AGN?	...	
SMM J123716.01+620323.3	2.053	...	28.1±3.2	19.5±2.4	9.7±2.2	...	QSO	...	AGN	2130±500	Multiple peaks and extended [O III] λ5007
SMM J123721.87+621035.3	0.979[c]	6.2±1.1	...	...	...	...	...	SB	...	...	
SMM J131201.17+424208.1	3.408	...	0.18±0.15	0.79±0.19	0.27±0.19	...	AGN	...	AGN?	...	
SMM J131215.27+423900.9	2.555	11.8±1.0	3.1±2.6	5.6±2.2	2.2±1.6	<0.23	QSO	...	AGN	2540±500	
SMM J131222.35+423814.1	2.560	...	12.1±4.5	5.5±2.5	2.6±2.5	2.0±1.5	QSO	...	AGN	2580±1000	
SMM J163639.01+405635.9	1.485[b]	7.3±0.7	0.7±0.5	2.5±0.5	1.1±0.4	...	SB	SB	Int	<1400	Extended Hα
SMM J163650.43+405734.5	2.380	14.2±1.5	2.3±0.6	27.0±2.1	6.8±1.3	14.0±0.8	Int	AGN	AGN	3720±500	Reevaluated after Smail et al. (2003)
MM J163655+4059	2.605	18.4±2.4	2.7±1.0	47.1±1.6	15.7±1.6	3.6±0.9	AGN	AGN	AGN	2410±600	Blue wings in Hβ and [O III] λ4959
SMM J163706.51+405313.8	2.373	7.4±1.4	0.6±0.3	5.7±0.6	1.9±0.6	1.0±0.3	AGN	AGN	AGN	1590±500	
SMM J221733.02+000906.0	0.926[c]	9.6±1.2	...	...	...	...	...	SB	...	...	
SMM J221733.79+001402.1	2.551	8.5±3.5	1.2±0.6	1.2±0.2	<0.5	0.7±0.3	SB	SB	AGN?	1860±600	
SMM J221737.39+001025.1	2.610[c]	20.7±6.0	0.6 ±0.4	6.0±0.4	1.2±0.4	...	SB	AGN	AGN	290±50	
SMM J04431+0210	2.510	1.6±0.1	<0.3	0.4±0.1	...	...	...	AGN?	AGN	...	Frayer et al. (2003)
SMM J14011+0252 (J1)	2.565	1.3±0.4	0.3±0.1	<0.2	<0.2[d]	0.4±0.1	SB	SB	SB	...	Motohara et al. (2005)
SMM J163658.19+410523.8	2.448	1.9±0.4	0.2±0.1	0.4±0.1	0.3±0.1	0.4±0.2	SB	SB	AGN	...	Simpson et al. (2004)
Composite (all)	...	...	1.0	$0.7^{+0.1}_{-0.1}$	$0.4^{+0.1}_{-0.1}$	$0.3^{+0.2}_{-0.1}$	...	...	...	3100±500	
Composite (QSO)	...	...	1.0	$0.36^{+0.33}_{-0.18}$	$0.19^{+0.21}_{-0.11}$	<0.12	...	...	...	3200±1000	
Composite (OPT-AGN)	...	...	1.0	$3.2^{+1.0}_{-0.6}$	$1.2^{+0.5}_{-0.3}$	$1.2^{+0.7}_{-0.4}$	...	...	...	1730±500	

[a] Based on [O III] λ5007 line measurement.
[b] Based on [O II] λ3727 line measurement.
[c] Based on Hα line measurement.
[d] Detected in Tecza et al. (2004).

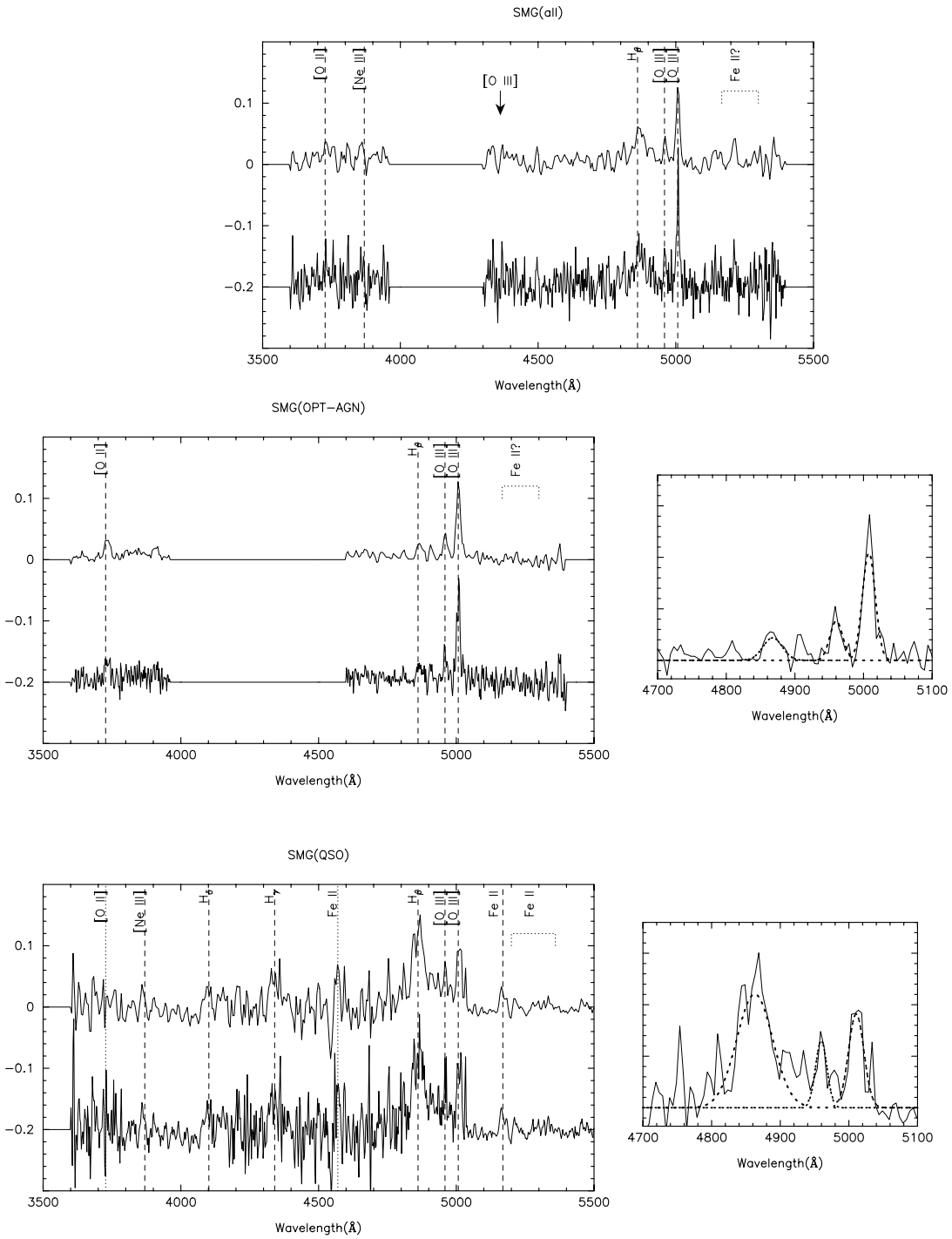

FIG. 3.—Stacked rest-frame spectra of subsets of galaxies in our sample. The top panel shows the spectrum of all of the sources in our sample, the middle left panel shows the combined spectrum of those sources classified as AGN based on their rest-frame optical spectra (except for those classified as QSO), and the bottom left panel is the combined spectrum of the three QSOs in our sample. The upper spectrum in each panel is smoothed to the instrumental resolution of Subaru OHS, and the lower one shows the raw stacked spectrum. The middle right and bottom right panels show the region around the Hβ and [O III] $\lambda\lambda$4959, 5007 emission lines with the best fit to these emission lines using three Gaussian profiles overlaid (*dotted lines*). The relative variation in the strength of [O III] $\lambda\lambda$4959, 5007 and Hβ is clearly visible between the different subsets. [*See the electronic edition of the Journal for a color version of this figure.*]

[N II]/Hα. This diagnostic plot, termed the BPT diagram, can be used to identify the source of gas excitation (Baldwin et al. 1981). Based on this diagram, we classify the spectra into three types: starburst (SB), intermediate (Int), or nonthermal (AGN), as listed in Table 2. We use the definitions from Kauffmann et al. (2003), which are derived for a large sample of local SDSS galaxies. We classify the sources between the boundary of Kauffmann et al. (2003) and the classical definition of Veilleux & Osterbrock (1987) as "Int." We also classify galaxies as "AGN" that have Hα and/or Hβ FWHM$_{\rm rest}$ greater than 1500 km s^{-1}, as it is difficult to understand the formation of such large line widths from gas motions in star-forming regions. This limit is also greater than the coarse spectral resolution of OHS ($\sim$1400 km s^{-1}). For comparison we also plot the emission-line flux ratios from local ULIRGs (Veilleux et al. 1999) and note that the SMGs in our sample occupy the same region of the diagnostic diagram as local ULIRGs. The lines show

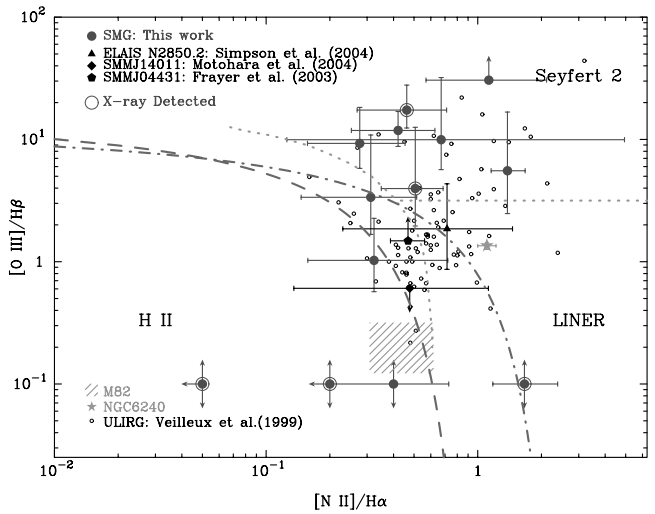

FIG. 4.—BPT classification diagram (Baldwin et al. 1981) for the galaxies in our sample. We plot the emission-line flux ratio [O III] λ5007/Hβ vs. [N II]/Hα for galaxies with strong Hα emission. In cases where there is no detection of either Hβ or [O III] λ5007, we set [O III] λ5007/Hβ as 1.0 and highlight the sources by plotting both lower and upper limits. Small open circles represent local ULIRGs from Veilleux et al. (1999). The dotted curve shows the division between AGNs and star-forming galaxies, and the dotted line is for separating Seyfert galaxies and LINERs, as defined by Veilleux & Osterbrock (1987). Dashed and dot-dashed curves are the division between AGNs and star-forming galaxies defined by Kauffmann et al. (2003) and Kewley et al. (2001), respectively. We also plot observations of three SMGs from the literature (Frayer et al. 2003; Simpson et al. 2004; Motohara et al. 2005). Large open circles denote X-ray–detected SMGs. For comparison we also plot the line ratios for NGC 6240 (Schmitt et al. 1996) and M82 (Shopbell & Bland-Hawthorn 1998), representing galaxies with (super)wind activity. Many of the galaxies in our sample show spectral line characteristics typical of AGNs. However, the reader should note that our sample is not representative of all SMGs due to the observational biases in our survey. [*See the electronic edition of the Journal for a color version of this figure.*]

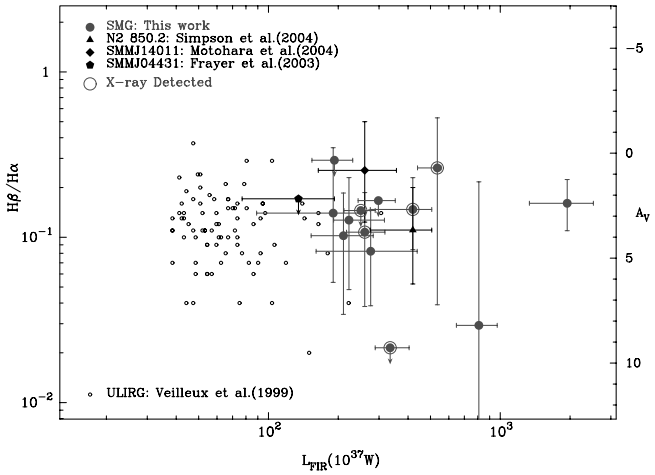

FIG. 5.—Hβ/Hα ratio as a function of far-infrared luminosity in our sample. The high-redshift ULIRGs display a similar Hβ/Hα ratio and range as typically lower luminosity systems at lower redshift. This suggests that they have comparable levels of dust obscuration to their optically detectable emission-line gas. The symbols are the same as in Fig. 4. [*See the electronic edition of the Journal for a color version of this figure.*]

various criteria for separating AGNs and the star-forming galaxies (see Fig. 4). It is clear that the majority, 8/13, of sources in our sample (including all but one, SMM J163639.01+405635.9, with all four emission lines detected) are classified as AGN based on these criteria. We reiterate that this subsample may be biased toward strong line emitters (due to the requirement to have detected lines in our low-resolution spectra) and so this is perhaps not a surprising result.

Moreover, we must interpret the BPT diagram with caution since "superwind" ejecta (shock-driven line-emitting gas) can occupy a very similar region to AGNs (Dopita & Sutherland 1995). To illustrate this possibility in more detail, we plot the emission-line ratio of the wind structure in M82 from a $\sim$1 kpc region (Shopbell & Bland-Hawthorn 1998) and in a 1.9×4.3 kpc^2 area of NGC 6240 (Schmitt et al. 1996). The former is indicative of a wind that is dominated by photoionization, and the latter illustrates the line ratios expected from shocks in a very dense environment. Some SMGs show very similar emission-line ratios to NGC 6240, although most of them have lower [N II]/Hα and higher [O III] λ5007/Hβ ratios. Further support for the wind scenario is that P Cygni features are seen in the rest-frame UV emission lines (Chapman et al. 2003a, 2005) of a significant fraction of the SMG population, supporting the presence of "winds" arising from the vigorous starburst activity. Indeed, the majority (6/8) of this subsample (with four detected emission lines) are classified as "SB" or "Int" from their rest-frame UV spectroscopic features (Chapman et al. 2005; Table 2). The power sources in SMGs are discussed further in § 4.2.

Looking at the individual sources in Figure 4, we note that SMM J123622.65+621629.7 has a very low [N II]/Hα (<0.05) emission line ratio and no detection of [O III] $\lambda\lambda$4959, 5007 and Hβ (see also Fig. 5 of Smail et al. 2004) with Hα/H$\beta > 4.25$ and [O III] λ5007/H$\alpha < 0.24$. This source is an interacting system of a relatively blue ($B - R \sim 0.2$) galaxy with an extremely red ($I - K = 4.0$) companion, where the latter is a hard X-ray source. While the slit was aligned along the major axis of the red X-ray source, it is possible that it also passed through the blue component and the line emission may be contaminated. To avoid biasing our sample, we have therefore eliminated this source from our subsequent analysis and discussion.

4.2. *Extinction and Hidden Star Formation*

SMGs are dusty systems with large dust masses, $>10^8\,M_\odot$, and high bolometric luminosities ($>10^{12}\,L_\odot$). The presence of large quantities of dust and its associated reddening may also explain the large discrepancies between the SFRs derived for SMGs from their far-infrared and Hα luminosities (Swinbank et al. 2004), which imply extinction in Hα of factors of $\sim$10–100. There are of course alternative explanations: that the bulk of the far-infrared emission originates from other sources that are too dusty to see even at rest-frame optical wavelengths, such as very highly obscured AGNs, or due to emission that falls outside of the slits used in the Hα measurements. However, the latter explanation is unlikely as these observations are based on radio-identified sources with precise positions ($\sim$0.″5; Chapman et al. 2005), and so it is unlikely that a major source of bolometric emission has been missed by the observations.

To investigate the internal reddening of SMGs (at least for those regions that are visible in the rest-frame optical), we plot the Hα/Hβ ratios as a function of their far-infrared luminosities in Figure 5. To calculate A_V, we use the reddening curve from Calzetti et al. (2000) and assume an intrinsic Hα/Hβ ratio of 3.0, which is between the values for typical Seyfert 2 galaxies and/or LINERs (3.1; Halpern & Steiner 1983; Gaskel & Ferland 1984) and those for star-forming galaxies (2.85; Veilleux & Osterbrock 1987). The observed Hα/Hβ ratio for the SMGs is typically 5–20, and the derived extinction spans $A_V = 1$–4 with a median value of 2.9 ± 0.5 (where the error comes from bootstrap resampling). This estimate is consistent with the results based on the spectral energy distribution (SED) fitting of optical to near-infrared photometric data (Smail et al. 2004) and slightly

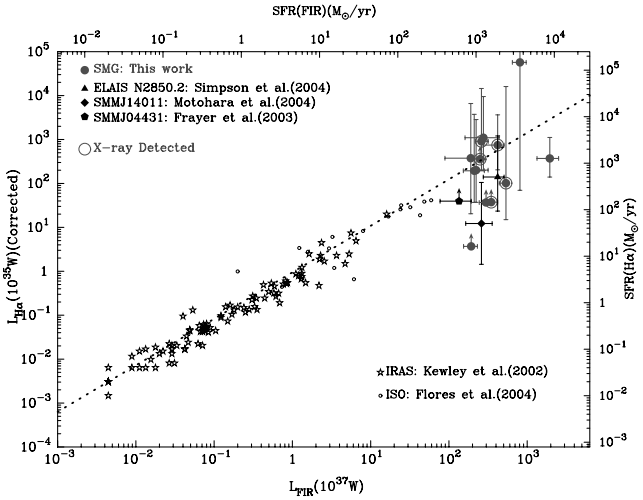

FIG. 6.—SFRs for our sample derived from the extinction-corrected Hα luminosities vs. those estimated from the far-infrared luminosities. For comparison we also plot samples of local *IRAS* galaxies (Kewley et al. 2002) and $z \sim 1$ *ISO* galaxies (Flores et al. 2004) as stars and open circles, respectively. The dotted line shows equality in the far-infrared and Hα SFRs. The high-redshift sources appear to extend the agreement between these two star formation indicators to higher SFRs, although there is considerable scatter (in part due to our use of Hα and Hβ observations taken with different instruments at different times). Nevertheless, the broad agreement between the Hα and far-infrared SFRs suggests that the bulk of the far-infrared luminosity in these galaxies is derived from star formation. [*See the electronic edition of the Journal for a color version of this figure.*]

higher than that derived from optical to mid-infrared SEDs (1.7 ± 0.3; Borys et al. 2005), where the latter did not include any contribution from thermally pulsed AGB stars in the model SEDs, which might lead to an underestimation of the reddening (Maraston et al. 2006).

In Figure 6 we compare the extinction-corrected SFRs derived from the Hα and far-infrared luminosities. The far-infrared luminosities come from Chapman et al. (2003b, 2004) based on SED model fitting to the observed 850 μm and 1.4 GHz fluxes at their known redshifts, assuming that the local far-infrared–radio correlation holds (Condon et al. 1991; Garrett 2002). We also include observations for local *Infrared Astronomical Satellite* (*IRAS*) galaxies (Kewley et al. 2002) and *Infrared Space Observatory* (*ISO*) galaxies (Flores et al. 2004). The typical A_V in these samples are $\sim$0.5 and $\sim$2.4, respectively. The extinction-corrected Hα luminosities for the *IRAS* and *ISO* galaxies are all calibrated in the same manner as for our SMG samples based on their Hα/Hβ ratio. The SFRs from the Hα and far-infrared luminosities are derived using the equations given in Kennicutt (1998).

The correlation between the far-infrared and reddening-corrected Hα luminosities (Fig. 6) appears to be relatively good, with a linear relation extending over 5 orders of magnitude in SFR, although with some scatter, with the most luminous SMGs in our sample having SFRs approximately an order of magnitude higher than those of the brightest *ISO* galaxies. The good agreement between the two SFRs when using the reddening-corrected Hα estimate confirms that the discrepancies between the SFRs seen in Swinbank et al. (2004) are in large part due to dust extinction and moreover that the bulk of the far-infrared luminosity in these galaxies is probably derived from star formation. We note that it is likely that slit losses and placement contribute to the scatter in these measurements as we are combining observations of Hβ and Hα from different telescopes and instruments. For example, our brightest far-infrared source, SMM J163650.43+405734.5 (N2 850.4), has a lower SFR measured from Hα than from the far-infrared. However, this galaxy is spatially extended and has a very complex structure in the rest-frame optical (Smail et al. 2003; Swinbank et al. 2005). It is therefore likely that our slit covered only a part of the Hα-emitting region. Finally, any remaining systematic offset between the two SFR estimates may be caused by the fact that our A_V estimates only reflect the reddening to the optically detectable gas and thus are not necessarily a good indicator of the total column toward the bolometric sources in these objects.

4.3. *Growing Black Holes in the SMGs*

4.3.1. *Spectral Similarity with Narrow-Line Seyfert 1 Galaxies*

SMGs are proposed to be the progenitors of present-day massive spheroidal galaxies because of their high SFRs and their large stellar, gas, and dynamical masses (Smail et al. 2004; Neri et al. 2003; Greve et al. 2005; Borys et al. 2005; Tacconi et al. 2006; Swinbank et al. 2006). Most massive galaxies in the local universe contain SMBHs (e.g., Ferrarese & Merritt 2000; Gebhardt et al. 2000; Marconi & Hunt 2003; Heckman et al. 2004). Equally an AGN appears to be almost universally present in SMGs: based on the extremely sensitive X-ray observations of the Chandra Deep Field–North (CDF-N), Alexander et al. (2003, 2005a, 2005b) found more than $\sim$75% of SMGs to be detected in hard X-rays, indicating that they contain an accreting SMBH. It is therefore interesting to estimate the mass of, and accretion rates onto, the central black holes of SMGs to constrain the coevolution of the SMBHs and the stellar masses of their surrounding bulge (Kawakatu et al. 2003; Granato et al. 2004).

The three sources classified as "QSO" in our sample have characteristics typical of local NLS1 galaxies: low [O III] λ5007/Hβ ratios ($\sim$0.5–1.8) and detectable Fe II emission in their individual and also composite spectra (Figs. 1 and 3). NLS1 galaxies are commonly interpreted as hosting rapidly growing SMBHs (Collin & Kawaguchi 2004), and hence the spectral similarities of these SMG QSOs with local NLS1 galaxies could imply comparable physical conditions in the accretion disk around the SMBH in the SMGs. However, the SMGs have $\mathrm{FWHM_{rest}} \sim 2000$–$2500$ km s^{-1} for their Balmer emission lines, and so they are not formally NLS1 galaxies because these line widths are higher than the definition used for NLS1 ($\mathrm{FWHM_{rest}}$ of Hβ of $<$2000 km s^{-1}). Nevertheless, it is worth noting that their Hβ $\mathrm{FWHM_{rest}}$ are close to the minimum for QSOs at $z \sim 0.1$–2.1 (Jarvis & McLure 2006) and narrower than the average of radio-quiet/radio-loud QSOs ($\sim$4800–6500 km s^{-1}). However, we caution that with the limited signal-to-noise ratio in our spectra we may underestimate the line widths, missing weak and broader line components. For instance, in the composite spectrum of SMG QSOs we estimate the $\mathrm{FWHM_{rest}}$ of the Hβ line as 3200 ± 1000 km s^{-1} using a single Gaussian fit. This is 500–1000 km s^{-1} broader than the mean of the individual spectra, suggesting that there may be an undetected broad component present in them. More secure estimates of the line widths would need either observations of stronger emission lines such as Hα, which are not available for these sources, or much deeper observations.

The $\mathrm{FWHM_{rest}}$ of the Balmer emission lines in those SMGs with AGN-like features (but omitting the three sources classified as "QSO") are 1000–3000 km s^{-1}. They are at least 1000–2000 km s^{-1} lower than the average FWHM of QSOs at $z \sim 0.1$–2.1 measured from Hβ and/or Mg II lines (Jarvis & McLure 2006), suggesting that the SMGs host lower mass SMBHs. This would support the claims of Alexander et al. (2005a, 2005b; see also Borys et al. 2005) based on Eddington-limited assumptions.

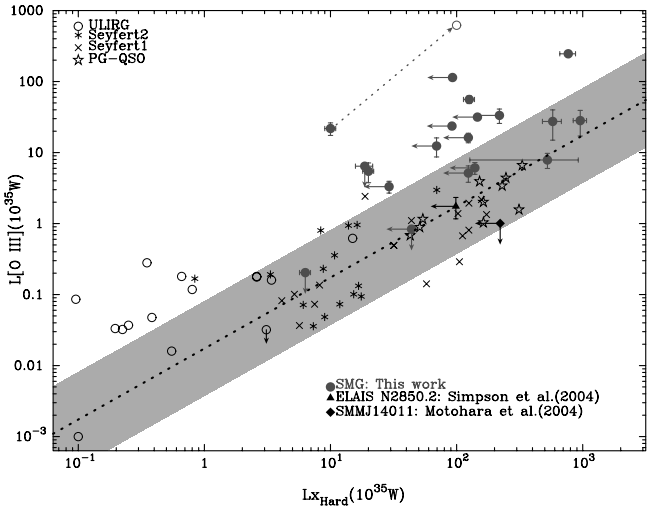

FIG. 7.—Hard X-ray luminosities vs. [O III] λ5007 luminosities for the galaxies in our sample. We also show similar observations for local ULIRGs (*triangles*), Seyfert 2 galaxies (*asterisks*), Seyfert 1 galaxies (*crosses*), and local QSOs (*stars*) for comparison. The dotted line shows the correlation between hard X-ray and [O III] λ5007 luminosities for Seyfert 2 galaxies derived by Mulchaey et al. (1994), and the shaded region shows the 3 σ error envelope for the sample. It should be noted that [O III] λ5007 and hard X-ray luminosities are not corrected for extinction or absorption in any of these samples. The open circle represents the data for SMM J123549.44+621536.8 (the only source with precise measurements for both corrections) with absorption-corrected [O III] λ5007 and hard X-ray luminosities, and the dotted arrow shows the amplitude of these corrections. The bulk of the sources in our sample show [O III] λ5007 luminosities significantly above those expected from their X-ray emission assuming the local relationship. As we show, applying extinction/absorption corrections to the data will not reduce this excess (as the correction moves objects parallel to the local relation). We suggest that this excess [O III] λ5007 emission arises from shocks within these galaxies. [*See the electronic edition of the Journal for a color version of this figure.*]

The similarities of the rest-frame optical spectral features of some SMGs to NLS1 galaxies imply rapid growth of the SMBH in the nuclei of SMGs. A total of 5/9 of the SMGs classified as "AGN" in our sample have relatively narrow $\mathrm{FWHM_{rest}}$ (up to $\sim$1600–3700 km s^{-1}) for their Hα or Hβ emission lines, and 3/5 show marginal Fe II emission. Therefore, the Eddington-limited accretion determined for local NLS1 galaxies may also be appropriate for SMGs. Assuming this, the measured line widths are then consistent with the estimate of the central BH masses derived from their X-ray luminosities under the assumption of Eddington-limited accretion ($\sim 10^6$–$10^8\ M_\odot$; Alexander et al. 2005b). However, this conclusion appears to be undermined by the fact that three of these NLS1-like SMGs display high (>10) [O III] λ5007/Hβ ratios that far exceed the NLS1 definition of [O III] λ5007/H$\beta < 3$; thus, these comparisons may not be appropriate.

4.3.2. *The Origin of* [O III] λ5007 *Excesses in SMGs*

To further test the claim that SMGs have small SMBH masses, we compare the [O III] λ5007 and hard X-ray luminosities. There is a well-studied correlation between the hard X-ray and the optical [O III] λ5007 emission line luminosities in local AGNs (e.g., Mulchaey et al. 1994). This correlation can be used to gauge the black hole masses and the accretion rates of AGNs within our sample.

In Figure 7 we show the hard X-ray versus [O III] λ5007 luminosities of the SMGs (uncorrected for any extinction/absorption). All 22 SMGs in our sample have hard X-ray coverage, but of varying depth (CDF-N, Alexander et al. 2003; CFRS 03hr, Waskett et al. 2004; SSA 13, Mushotzky et al. 2000; SSA 22, Basu-Zych & Scharf 2004; ELAIS N2, Manners et al. 2003). We adopt the hard X-ray fluxes from these observations, although 9/22 of them yield only the upper limits. For comparison, we also plot observations of local ULIRGs (Ptak et al. 2003; Franceschini et al. 2003), as well as Seyfert 1 and Seyfert 2 galaxies and the PG QSOs, representative of more luminous type 1 AGNs (Alonso-Herrero et al. 1997; Mulchaey et al. 1994). All of these comparison samples are the *observed* luminosities: there are no extinction corrections applied to either the X-ray or [O III] λ5007 measurements.

Figure 7 also shows the relation for Seyfert 2 galaxies suggested by Mulchaey et al. (1994). Compared to the QSOs and Seyfert 1 galaxies, which are selected to represent unabsorbed hard X-ray sources, the majority of our SMGs are typically an order of magnitude brighter in [O III] λ5007 for a given hard X-ray luminosity. We note that a similar excess of [O III] λ5007 emission is also seen in local ULIRGs.

Could this apparent excess be due to absorption/extinction? The typical hydrogen column densities to the AGNs in SMGs have been determined by Alexander et al. (2005a), yielding $N_{\mathrm{H}} \sim 10^{23}$–$10^{24}$ cm^{-2}, with corrections to their hard X-ray luminosities of 2.5–20 times. Equally, the typical [O III] λ5007 luminosity correction, adopting the extinction estimated from the Balmer decrement, $A_V \sim 2.9$, is also approximately a factor of 10: $F_{[\mathrm{O\ III}]\lambda 5007_{\mathrm{corrected}}} = F_{[\mathrm{O\ III}]\ \lambda 5007_{\mathrm{obs}}}[(\mathrm{H}\alpha/\mathrm{H}\beta)/(\mathrm{H}\alpha_0/\mathrm{H}\beta_0)]^{2.94}$, where $\mathrm{H}\alpha_0/\mathrm{H}\beta_0$ is assumed to be 3.0 (see Bassani et al. 1999). Unfortunately, we have only one source (SMM J123549.44+621536.8) with reliable estimates of the H I column density and reddening correction that has 10 times and 28.5 times corrections to the hard X-ray and [O III] λ5007 luminosities, respectively, and with corrected luminosities of 1×10^{44} and 6.2×10^{44} ergs s^{-1}, respectively (Fig. 7).

As the extinction corrections for [O III] λ5007 and hard X-ray luminosities run parallel to the trend in Figure 7, the [O III] λ5007 excess cannot be explained by a simple reddening effect. We also caution that the reddening corrections applied to the [O III] λ5007 fluxes are uncertain since [O III] λ5007 may arise in external shocks that suffer much less extinction than the Hα/Hβ ratio suggests. We also note that the apparent [O III] λ5007 excess could arise simply due to the relatively shallow X-ray coverage in several of our fields where the sources only have upper limits on their hard X-ray fluxes. However, the fact that 3/4 sources with [O III] λ5007 and hard X-ray detections from the CDF-N, which has by far the best X-ray data, show the excess provides good evidence for the reality of this feature.

While some of the [O III] λ5007 flux we see arises from the obscured AGN, we suggest that the excess [O III] λ5007 flux arises, at least in part, from shock-induced ("superwind") activity. There are some cases of plausible superwind-driven [O III] λ5007 excesses seen in our SMG sample as seen by the structured [O III] λ5007 line profiles (asymmetric/broad/multipeaked) and the spatially extended emission (Figs. 1 and 2; see also Smail et al. 2003).

In order to examine the possibility that shock-induced gas causes the excess [O III] λ5007 emission, we first search for the signature of shock-excited nebular emission using the simple criterion of [N II] λ6583/H$\alpha \geq 1$ and [S II] $\lambda\lambda$6716, 6731/H$\alpha \geq 0.5$. Using the line ratios from the stacked spectrum of SMGs in Swinbank et al. (2004), we find that they lie outside of this shock-induced criterion. However, this criterion is only valid for the shocks with large outflow velocities and a relatively weak starburst radiation field (Veilleux et al. 2005) and therefore may not be applicable to the SMGs. Another test is to use the line ratios of [O III] $\lambda\lambda$4959, 5007/[O III] λ4363 and/or [N II] $\lambda\lambda$6548, 6583/[N II] λ5755, which can be used to estimate the temperature of

the nebular gas. These ratios will provide robust estimates of electron temperature of the emission nebulae, yielding high ($\sim$30,000 K) temperatures if the gas is ionized mainly by shocks (as in the Cygnus Loop) and lower temperature ($\sim$15,000 K) for photoionization-dominated clouds seen in star-forming regions (Osterbrock 1989). As these methods rely on measurements of relatively weak emission lines [O III] λ4363 and [N II] λ5755, only our composite spectra have sufficient signal-to-noise ratio to be useful. From the composite spectrum in Figure 3 and also from the total SMG composite spectrum in Swinbank et al. (2004), we derive an upper limit on [O III] $\lambda\lambda$4959, 5007/[O III] λ4363 $<$ 37.2 and [N II] $\lambda\lambda$6548, 6583/[N II] λ5755 $<$ 23.6. Both ratios imply an upper limit to the electron temperature of less than 20,000 K. This is consistent with the expected temperature in photoionization-dominated clouds (with an electron density of $\sim 10^3$–10^4 cm^{-2}). If the electron density is higher than this, collisional de-excitation begins to play a role and the estimated temperature is reduced. These results would appear to rule out the dominance of shock excitation similar to that seen in galactic supernova remnants.

As described in Dopita & Sutherland (1995), the optical line ratios of Seyfert 2 galaxies can also be explained by fast (300–500 km s^{-1}) shocks, if the precursor H II regions in front of the shock absorb most of the UV photons generated by the shocks. The calculated electron temperature is $\sim$17,000 K for this "shock + precursor" model from Dopita & Sutherland (1995), which is consistent with the limit on the electron temperatures in SMGs estimated from our [N II] and [O III] emission line ratios. Thus, there is a plausible origin for the [O III] λ5007 excess we see compared to typical AGNs: shocks associated with supernova explosions in relatively dense gas environments, where the precursor H II clouds are still present. Thus, we suggest that those sources with high ($\sim$5–10) [O III] λ5007/Hβ ratios and broad ($\sim$2000 km s^{-1}) FWHM of Hβ lines can be explained by a combination of an NLS1-type AGN residing in an environment of shocks associated with supernova explosions in relatively dense gas. This would explain all of their observable properties, including the high [O III] λ5007/Hβ ratios (Dopita & Sutherland 1995).

5. CONCLUSIONS

Using near-infrared spectroscopy, we have observed the redshifted Hβ, [O III] $\lambda\lambda$4959, 5007, and [O II] λ3727 emission lines in a sample of 22 ULIRGs at high redshifts. Twenty of the sources in our sample are SMGs at $z \sim 1.0$–3.5. Combining our observations with previous studies of the Hα and [N II] emission from these galaxies and also with observations of their hard X-ray and far-infrared emission, we have placed constraints on the physical properties of this population. We conclude the following:

1. A majority of our sample (14/22) have spectra that are classified as "AGN" or "QSO" based on several rest-frame optical spectroscopic diagnostics. Specifically, for those sources with detections of the four emission lines necessary to construct a BPT diagram, 8/9 are classified as "AGN." It should be noted that there is no confirmed pure starburst galaxy in our sample, although several sources show intermediate spectral properties. This is likely to be caused by our sample selection, which is biased toward galaxies with bright near-infrared magnitudes and also to those exhibiting strong line emission. Thus, we caution that our results should not be taken as representative of the whole SMG population.

2. Using the Hα/Hβ flux ratio, we are able to estimate the internal extinction in our SMGs. We measure a median extinction of $A_V = 2.9 \pm 0.5$, which is similar to the extinction measured in local ULIRGs. This value is also consistent with the estimates from the SED fitting in the rest-frame UV/optical that are derived under the assumption of a dominant dust-reddened young starburst (Smail et al. 2004).

3. We compare the SFRs derived from the dust-extinction–corrected Hα luminosities with those derived from the far-infrared luminosities and find reasonable consistency between these for most of the SMGs in our sample. The fact that the corrected Hα-derived SFRs correspond closely to those estimated from the far-infrared suggests that star formation is the major contributor to the far-infrared luminosities in SMGs.

4. At least 11/19 of the SMGs in our sample show a clear excess in the ratio of their [O III] λ5007 to X-ray luminosities relative to values for local AGNs. The five sources with the highest [O III] λ5007/Hβ ratios (>10), which are classified as "AGN" from our spectral diagnostics, show this [O III] λ5007 excess. One possible explanation for the [O III] λ5007 excess is that it is produced by "Compton thick" AGNs. However, this is inconsistent with the column density measurements (N_H) from fitting of the X-ray spectra for the sources in CDF-N, and we argue that this is unlikely in most SMGs. Instead, we suggest that the most plausible cause of the [O III] λ5007 excess is shock-induced emission arising from vigorous star formation (superwind activity). This scenario is supported in several galaxies by spatially extended and/or distorted/multiple [O III] λ5007 emission line profiles. Furthermore, using limits on the electron temperatures from [O III] and [N II] emission line ratios, we can explain the excess [O III] λ5007 emission as arising from shocks in dense regions within these systems.

5. The Balmer line widths in 9/22 sample galaxies exhibit broad emission components with relatively small FWHMs ($\sim$1500–3700 km s^{-1}). Three of them are classified as "QSO" but have smaller Hβ FWHM (2100–2600 km s^{-1}) than are typical for QSOs. They also have lower [O III] λ5007/Hβ ratios and relatively strong Fe II emission, both of which are characteristics of local NLS1 galaxies. Among the other six sources, only one shows a low [O III] λ5007/Hβ ratio, and four show high [O III] λ5007/Hβ ratios (larger than seen in NLS1 galaxies). However, the high [O III] λ5007/Hβ ratios may arise from [O III] λ5007 excesses due to shock excitation, and hence removing this contribution would yield lower ratios more consistent with NLS1 classification. Several of these sources also have tentative evidence for Fe II emission, again characteristic of NLS1 galaxies. Thus, once account is taken of the potential contribution from shocks to the excess [O III] λ5007 emission, there appear to be close similarities between SMGs and NLS1 galaxies. The spectral classification of SMGs as NLS1 galaxies may then indicate (as has been claimed for local NLS1 galaxies) that SMGs have low-mass black holes that are rapidly growing at high accretion rates (Alexander et al. 2005a, 2005b; Borys et al. 2005). Deeper spectroscopic observations are essential to search for any obscured broad Balmer lines that might indicate larger SMBH masses and confirm the presence of Fe II lines that are common in the NLS1 galaxies.

Summarizing our results, we conclude that our sample of SMGs contains a population of vigorously star-forming galaxies with high SFRs and strong extinction. The activity in these systems is driving shocks through the dense gas reservoirs they contain, and some of this material is being expelled from the galaxies. In addition, many of our sources show evidence for low-mass, but rapidly growing, SMBHs. These results confirm the critical place of the submillimeter-bright phase in defining the properties of massive galaxies forming at high redshifts.

We are grateful to Michael Balogh, Bob Nichol, Chris Miller, and Dave Alexander for providing invaluable information and discussions. T. T. and K. S. are also grateful to all staffs of the Subaru Telescope, especially Kentaro Aoki and Takuya Fujiyoshi for support on our Subaru/OHS observation. We also thank the anonymous referee for various comments and suggestions that helped to improve our manuscript. I. R. S. acknowledges support from the Royal Society. J. E. G. acknowledges support from a PPARC postgraduate studentship. A. M. S. acknowledges a PPARC fellowship.

REFERENCES

Alexander, D., Smail, I., Bauer, F., Chapman, S. C., Blain, A. W., & Ivison, R. 2005a, ApJ, 632, 736
———. 2005b, Nature, 434, 738
Alexander, D. M., et al. 2003, AJ, 126, 539
Alonso-Herrero, A., Ward, M. J., & Kotilainen, J. K. 1997, MNRAS, 288, 977
Baldwin, J. A., Phillips, M. M., & Terlevich, R. 1981, PASP, 93, 5
Barger, A. J., Cowie, L. L., Sanders, D. B., Fulton, E., Taniguchi, Y., Sato, Y., & Okuda, H. 1998, Nature, 394, 248
Bassani, L., Dadina, M., Maiolino, R., Salvati, M., Risaliti, G., Della Cesa, R., Matt, G., & Zamorani, G. 1999, ApJS, 121, 473
Basu-Zych, A., & Scharf, C. 2004, ApJ, 615, L85
Bautz, M. W., Malm, M. R., Baganoff, F. K., Ricker, G. R., Canizares, C. R., Brandt, W. N., Hornschemeier, A. E., & Garmire, G. P. 2000, ApJ, 543, L119
Blain, A. W., Chapman, S. C., Smail, I., & Ivison, R. J. 2004, ApJ, 611, 52
Blain, A. W., Smail, I., Ivison, R. J., & Kneib, J.-P. 1999, MNRAS, 302, 632
Blain, A. W., Smail, I., Ivison, R. J., Kneib, J.-P., & Frayer, D. T. 2002, Phys. Rep., 369, 111
Borys, C., Smail, I., Chapman, S. C., Blain, A. W., Alexander, D. M., & Ivison, R. J. 2005, ApJ, 635, 853
Calzetti, D., Armus, L., Bohlin, R. C., Kinney, A. L., Koornneef, J., & Storchi-Bergmann, T. 2000, ApJ, 533, 682
Chapman, S. C., Blain, A. W., Ivison, R. J., & Smail, I. 2003a, Nature, 422, 695
Chapman, S. C., Blain, A. W., Smail, I., & Ivison, R. 2004, ApJ, 614, 671
———. 2005, ApJ, 622, 772
Chapman, S. C., Windhorst, R., Odewahn, S., Yan, H., & Conselice, C. 2003b, ApJ, 599, 92
Collin, S., & Kawaguchi, T. 2004, A&A, 426, 797
Condon, J. J., Anderson, M. L., & Helou, G. 1991, ApJ, 376, 95
Cowie, L. L., Barger, A. J., & Kneib, J. P. 2002, AJ, 123, 2197
Desai, V., et al. 2006, ApJ, 641, 133
Dopita, M. A., & Sutherland, R. S. 1995, ApJ, 455, 468
Fabian, A. C., et al. 2000, MNRAS, 315, L8
Ferrarese, L., & Merritt, D. 2000, ApJ, 539, L9
Flores, H., Hammer, F., Elbaz, D., Cesarsky, C. J., Liang, Y. C., Fadda, D., & Gruel, N. 2004, A&A, 415, 885
Franceschini, A., et al. 2003, MNRAS, 343, 1181
Frayer, D. T., Armus, L., Scoville, N. Z., Blain, A. W., Reddy, N. A., Ivison, R. J., & Smail, I. 2003, AJ, 126, 73
Garrett, M. A. 2002, A&A, 384, L19
Gaskell, C. M., & Ferland, G. I. 1984, PASP, 96, 393
Gebhardt, K., et al. 2000, ApJ, 543, L5
Goodrich, R. W. 1989, ApJ, 342, 224
Granato, G. L., De Zotti, G., Silva, L., Bressan, A., & Danese, L. 2004, ApJ, 600, 580
Greve, T. M., Ivison, R. J., Bertoldi, F., Stevens, J. A., Dunlop, J. S., Lutz, D., & Carilli, C. L. 2004, MNRAS, 354, 779
Greve, T. M., et al. 2005, MNRAS, 359, 1165
Halpern, J. P., & Steiner, J. E. 1983, ApJ, 269, L37
Hawarden, T. G., Leggett, S. K., Letawsky, M. B., Ballantyne, D. R., & Casali, M. 2001, MNRAS, 325, 563
Heckman, T. M., Kauffmann, G., Brinchmann, J., Charlot, S., Tremonti, C., & White, S. 2004, ApJ, 613, 109
Holland, W. S., et al. 1999, MNRAS, 303, 659
Houck, J. R., et al. 2005, ApJ, 622, L105
Hughes, D. H., et al. 1998, Nature, 394, 241
Ivison, R. J., et al. 2006, ApJ, in press (astro-ph/0607271)
Iwamuro, F., Motohara, K., Maihara, T., Hata, R., & Harashima, T. 2001, PASJ, 53, 355
Iye, M., et al. 2004, PASJ, 56, 381
Jarvis, M. J., & McLure, R. J. 2006, MNRAS, 369, 182
Kauffmann, G., et al. 2003, MNRAS, 346, 1055
Kawakatu, N., Umemura, M., & Mori, M. 2003, ApJ, 583, 85
Kennicutt, R. C., Jr. 1998, ARA&A, 36, 189
Kewley, L., Dopita, M., Sutherland, R., Heisler, C., & Trevena, J. 2001, ApJ, 556, 121
Kewley, L., Geller, M. J., Jansen, R. A. & Dopita, M. A. 2002, AJ, 124, 3135
Kovacs, A., Chapman, S. C., Dowell, C. D., Blain, A. W., Ivison, R. J., Smail, I., & Phillips, T. G. 2006, ApJ, 650, 592
Ledlow, M. J., Smail, I., Owen, F. N., Keel, W. C., Ivison, R. J., & Morrison, G. E. 2002, ApJ, 577, L79
Lilly, S. J., Eales, S. A., Gear, W. K. P., Hammer, F., Le Fevre, O., Crampton, D., Bond, J. R., & Dunne, L. 1999, ApJ, 518, 641
Lutz, D., Yan, L., Armus, L., Helou, G., Tacconi, L. J., Genzel, R., & Baker, A. J. 2005, ApJ, 632, L13
Manners, J. C., et al. 2003, MNRAS, 343, 293
Maraston, C., et al. 2006, ApJ, submitted (astro-ph/0604530)
Marconi, A., & Hunt, L. K. 2003, ApJ, 589, L21
Motohara, K., et al. 2002, PASJ, 54, 315
———. 2005, AJ, 129, 53
Mulchaey, J. S., Koratkar, A., Ward, M. J., Wilson, A. S., Whittle, M., Antonucci, R. R. J., Kinney, A. L., & Hurt, T. 1994, ApJ, 436, 586
Mushotzky, R. F., Cowie, L. L., Barger, A. J., & Arnaud, K. A. 2000, Nature, 404, 459
Neri, R., et al. 2003, ApJ, 597, L113
Osterbrock, D. E. 1989, Astrophysics of Gaseous Nebulae and Active Galactic Nuclei (Mill Valley: University Science Books)
Osterbrock, D. E., & Pogge, R. W. 1985, ApJ, 297, 166
Ptak, A., Heckman, T., Levenson, N. A., Weaver, K., & Strickland, D. 2003, ApJ, 592, 782
Schmitt, H. R., Bica, E., & Pastoriza, M. G. 1996, MNRAS, 278, 965
Scott, S., et al. 2002, MNRAS, 331, 817
Shopbell, P. L., & Bland-Hawthorn, J. 1998, ApJ, 493, 129
Simpson, C., Dunlop, J. S., Eales, S. A., Ivison, R. J., Scott, S. E., Lilly, S. J., & Webb, T. M. A. 2004, MNRAS, 353, 179
Smail, I., Chapman, S. C., Blain, A. W., & Ivison, R. 2004, ApJ, 616, 71
Smail, I., Chapman, S. C., Ivison, R. J., Blain, A. W., Takata, T., Heckman, T. M., Dunlop, J. S., & Sekiguchi, K. 2003, MNRAS, 342, 1185
Smail, I., Ivison, R. J., & Blain, A. W. 1997, ApJ, 490, L5
Smail, I., Ivison, R. J., Blain, A. W., & Kneib, J.-P. 2002, MNRAS, 331, 495
Soucail, G., Kneib, J.-P., Bezecourt, J., Metcalfe, L., Altieri, B., & Le Borgne, J. F. 1999, A&A, 343, L70
Swinbank, M., Chapman, S. C., Smail, I., Lindner, C., Borys, C., Blain, A. W., Ivison, R., & Lewis, G. F. 2006, MNRAS, 371, 465
Swinbank, M., Smail, I., Chapman, S. C., Blain, A. W., Ivison, R., & Keel, W. C. 2004, ApJ, 617, 64
Swinbank, M., et al. 2005, MNRAS, 359, 401
Tacconi, L., et al. 2006, ApJ, 640, 228
Tecza, M., et al. 2004, ApJ, 605, L109
van Dokkum, P. G., et al. 2004, ApJ, 611, 703
Veilleux, S., Cecil, G., & Bland-Hawthorn, J. 2005, ARA&A, 43, 769
Veilleux, S., Kim, D.-C., & Sanders, D. B. 1999, ApJ, 522, 113
Veilleux, S., & Osterbrock, D. E. 1987, ApJS, 63, 295
Waskett, T. J., Eales, S. A., Gear, W. K., McCracken, H. J., Brodwin, M., Nandra, K., Laird, E. S., & Lilly, S. 2004, MNRAS, 350, 785
Willott, C., et al. 2003, MNRAS, 339, 397
Yan, L., et al. 2005, ApJ, 628, 604